Lawrence Berkeley National Laboratory

Title
Development and Prospects of Halide Perovskite Single Crystal Films

Permalink
https://escholarship.org/uc/item/3mx4m3vs

Journal
Advanced Electronic Materials, 8(4)

ISSN
2199-160X

Authors
Gao, Wenxiu
Zhang, Zhuolei
Xu, Rukai
et al.

Publication Date
2022-04-01

DOI
10.1002/aelm.202100980

Peer reviewed

Development and prospect of halide perovskite single crystal films

Wenxiu Gao, Zhuolei Zhang, Rukai Xu, Emory M. Chan,* Guoliang Yuan,* and Jun-Ming Liu

Dr. W. Gao, R. Xu, Prof. G. Yuan
School of Materials Science and Engineering
Nanjing University of Science and Technology
Nanjing, Jiangsu 210094, P. R. China
yuanguoliang@njust.edu.cn
Dr. Z. Zhang, Prof. E. Chan
Molecular Foundry
Lawrence Berkeley National Laboratory
Berkeley, California 94720, United States
emchan@lbl.gov
Prof. J.-M. Liu
National Laboratory of Solid State Microstructures
Nanjing University
Nanjing 210093, China

Halide perovskite single crystal (HPSC) films have demonstrated extraordinary performance in solar cells, photodetectors, and lighting applications, owing to the high carrier mobility, long carrier diffusion length, tunable bandgap, and large light absorption coefficients of these materials. Here, we review the recent development of the major HPSC thin films systematically, including $MAPbI_3$, α-$FAPbI_3$, $MAPbBr_3$, $CsPbBr_3$, with special emphasis on different classes of fabrication methods and thin-film characteristics. Finally, the conclusion and prospects in this field are discussed in detail. We anticipate that the HPSC thin films will lead to a compelling future for the rising electronic applications.

1. Introduction

Semiconductor thin films comprised of single crystals exhibit exceptionally low trap density, nearly perfect translational symmetry and high chemical purity, allowing them to play an essential role in the development of semiconductor and microelectronic industries.[1, 2] For example, silicon (Si) epitaxial films are grown on Si single crystals to fabricate transistors,

which are the basic unit of the Si-based Central processing units (CPUs) , memory modules, and many other electronic devices.[3, 4] The p-type doping of GaN single-crystal films on aluminum oxide (Al_2O_3) substrate enables high brightness blue light-emitting diodes (LED) and blue-light laser devices.[5, 6] Furthermore, gallium arsenide (GaAs), indium phosphide (InP) and other single-crystal semiconductor films are model materials in modern microelectronic industries.[7, 8]

Beyond these canonical systems, there is high demand to expand these methods to preparing single crystal thin films of emerging semiconductors such as halide perovskite ABX_3 materials (e.g., $MAPbX_3$, $FAPbX_3$ and $CsPbX_3$, where MA^+ is $CH_3NH_3^+$, FA^+ is $CH(NH_2)_2^+$ and $X^- = Cl^-$, Br^-, or I^-.[9, 10] ABX_3 generally describes the formula of the canonical perovskite unit cell, in which A^+ represents either an organic cation, such as MA^+, or an inorganic one, such as Cs^+; B indicates a divalent metal cation, such as Pb^{2+} and Sn^{2+}; and X^- stands for a halogen anion, such as Cl^-, Br^-, or I^-.[11] **Figure 1**a illustrates the three-dimensional halide perovskite crystal structure.[12] Corner-sharing metal halide BX_6 octahedral form the framework of the cubic perovskite crystal structure. The A^+ cation sits in the intersticial spaces of this metal halide framework, with hydrogen bonding possible between A^+ and X^- ions.[13] Although variants of perovskite material structures exist, they conform to limitations in the size, charge balance, shape and other factors to maintain the stability even with distortion in the crystal structure. The degree of distortion is indicated by Goldschmidt's tolerance factor t in **Equation 1**:

$$t = \frac{r_A + r_X}{\sqrt{2}(r_B + r_X)}$$

(1)

where r_A, r_B, r_X are the radii of A^+, B^+ and X^-, respectively.[14]
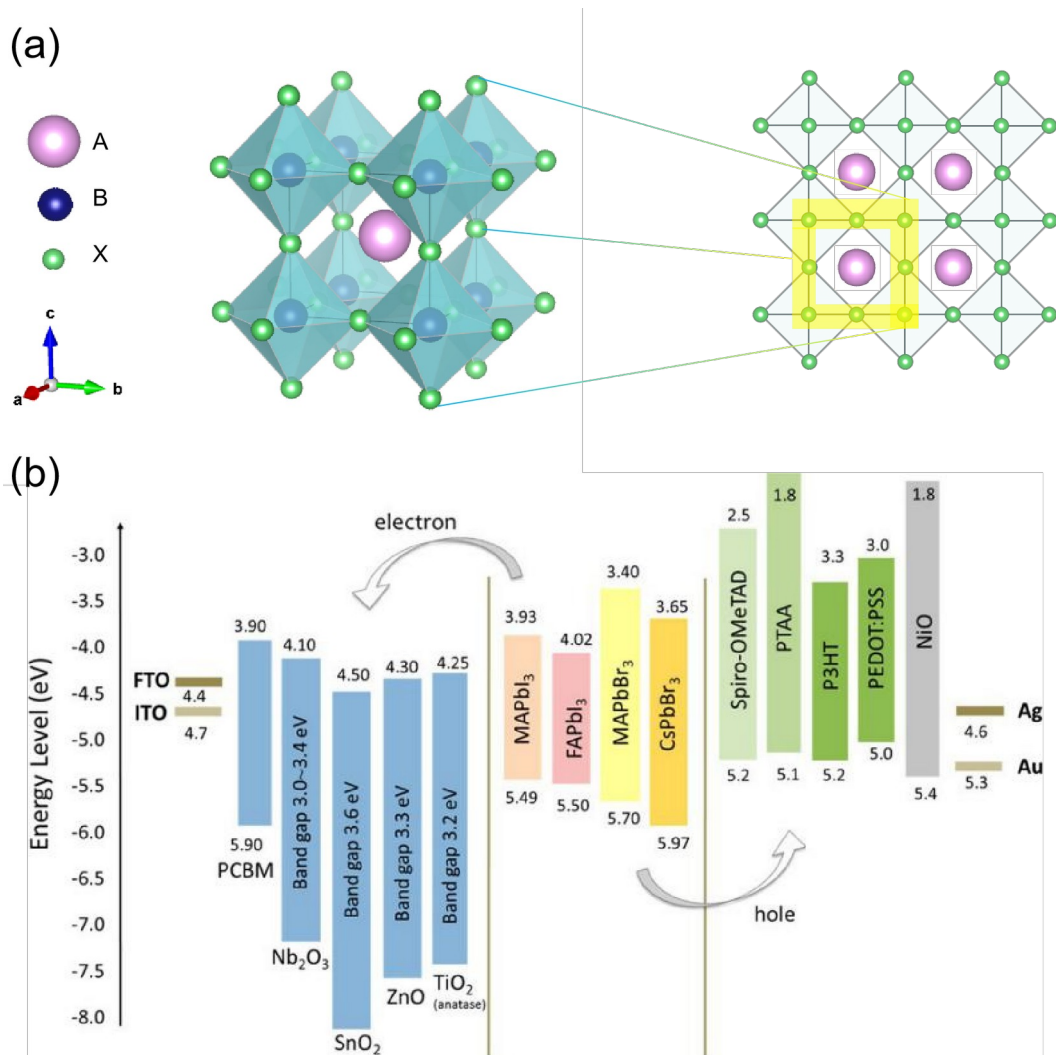
Figure 1. a) ABX$_3$ crystal structure of halide perovskites. Violet spheres indicate the monovalent A$^+$ cation standing in the octahedra space which is made up of B^{2+} cations in the center and X$^-$ anions at the vertex, respectively. Blue spheres depict B$^+$ cations and green spheres are X$^-$ halogen anions. b) Band edge positions of representative electron transport layer (ETL) materials (blue), halide perovskite absorbers (yellow), and hole transport layer (HTL) materials (green), realizing their potential in solar cell industries. Reproduced with permission.[12] Copyright 2019, American Chemical Society.

Even in conventional polycrystalline thin films and solids, MAPbX$_3$ features the advantages of appropriate bandgap (1.55-2.2 eV), exceptionally long carrier diffusion length, [15] high mobility, high absorption, and easy preparation.,[16] driving many improvements in perovskite photovoltaic devices as the absorber materials.[17, 18] The canonical halide perovskite material, MAPbI$_3$ was first applied by Kojima et al. as the light-absorbing layer in dye-sensitized solar cells in 2009.[19] Functional halide perovskite materials have been applied

to solar cells, field-effect transistors,[20, 21] LEDs,[22, 23] photodetectors, and photocatalytic devices.[24, 25] The record power conversion efficiency of perovskite single-crystal films based solar cells has reached 21.09%, which was obtained on 20-μm-thick single-crystal $MAPbI_3$ perovskite [26] Doping $MAPbI_3$ perovskite materials with alkali metals has been demonstrated to further improve the optical and electronic tunability of these materials.[27, 28] Single-crystal $MAPbI_3$ produced through low-temperature crystallization has been used by Alsalloum et. al. [29] to fabricate highly efficient inverted perovskite solar cells. Another candidate among the chief halide perovskite materials, $CsPbX_3$, also exhibits superior emitting properties[30, 31] and is more stable than $MAPbX_3$,[32] leading to applications in photodetectors and LED devices.[33, 34] For example, Li et. al. demonstrated that controlling surface ligand density on $CsPbBr_3$ perovskite quantum dots can lead to a 50-fold improvement external quantum efficiency in light-emitting diodes incorporating the nanoparticles.[35]

In order to improve device performance and efficiency, the morphology of traditional polycrystalline halide perovskite materials must be enhanced.[36] HPSC thin films, compared with their polycrystalline counterparts, offer tunable dimensions, enhanced uniformity and stability, minimum grain boundaries, and orientation-dependent transport behavior.[37, 38] Unfortunately, due to the uncontrollable nucleation of the deposited materials, most perovskite films produced thus far are polycrystalline with many small grains separated by grain boundaries. The high density of surface traps at these grain boundaries is one of the primary reasons for the relatively low performance of perovskite devices based on polycrystalline films versus those based on single-crystal films. Perovskite single-crystal films present a promising strategy to address these issues[39, 40] since the single crystals minimize internal grain boundaries. [41, 42] In principle, converting HSPC thin film devices to use HPSC films should reduce internal defects and carrier scattering.[43, 44] Developing robust methods for

4

producing such films is an essential prerequisite for fabricating semiconductor devices suitable for industrial applications.[45]

However, the adoption of HPSC thin films has been limited due two factors.First, it is difficult to reduce the thickness of the single-crystal bulk materials below 1 μm in a cost-effective way.[46] Thus, most high-quality as-grown single-crystal thin films are grown epitaxially on conventional semiconductor materials, although further development of alternate routes HSPC films are needed. Second, despite their minimization of internal defects, HPSCs can exhibit high recombination rates due to the high density of traps at their surfaces, which comprise most of the volumes in thin films. This extreme recombination is currently a major obstacle to the improvement of PCEs of HPSC-based photovoltaic applications.[47, 48] Simulations suggest that the defect density and extreme recombination at the surfaces of single crystals influence charge transport properties more than the bulk defect density.[49] Minimizing surface traps by tuning the growth and post-growth surface treatments is instrumental in overcoming rapid recombination in HPSC films.[47]

Here we review the recent development of the major fabrication methods, growth mechanism and properties of popular HPSC films as well as their current challenges. Hybrid organic-inorganic and fully inorganic lead halide perovskites thin films, are discussed. In particular, canonical perovskite thin films of $MAPbI_3$, $MAPbBr_3$, $CsPbBr_3$ are highlighted because they are widely investigated and utilized in a wide range of applications.[50, 51] Finally, based on the current challenges existed in the field, we present an outlook for the further advancement of HPSC thin films.

2. Growth of ABX_3 halide perovskite single-crystal films

ABX_3 HPSC films must be produced using methods that can controllably grow highly anisotropic materials with nanoscale thicknesses while mainting crystalline order across

5

macroscale lateral dimensions. To meet these requirements, substantial progress has been made in the growth halide perovskite single crystal (HPSC) thin films.[52, 53] These growth methods, targeted to specific characteristics and applications,[40, 54] mainly include (1) epitaxial growth of HPSCs on crystalline substrates, and (2) lateral growth of HPSC films on arbitrary substrates.

2.1 Epitaxial growth of HPSCs.

One of the most common methods for producing HPSCs is to grow them epitaxially on another single crystal substrate, such that the lattice of the substrate acts as a template for maintaining the order of the HPSC film. This approach has been used to grow champion HPSC thin films of, e.g., MAPbI$_3$, CsPbBr$_3$, and α-FAPbI$_3$.[55, 56] The technique has been used to advance film fabrication methods, enhance properties of HSPCs, and develop applications in photoelectronic devices.[57, 58]

At the current stage, one critical challenge facing the growth of HPSC films is to identify compatible substrates whose lattices are matched to the crystal structure of the perovskite material, as required for epitaxial growth.[59] The lattice mismatch (ε) between the film and the substrate can be calculated using **Equation 2**:[60]

$$\varepsilon = \frac{d_{film} - d_{substrate}}{d_{substrate}} \times 100\%$$

(2)

Here, d_{film} denotes the interplanar spacing of the thin film and the $d_{substrate}$ denotes that of the substrate. An ε of > 4% usually results in incompatibility between the film and substrate. Other factors, such as the different chemical potential or interfacial energy between the films and the substrates, can also promote or suppress single crystal thin film growth.[61]

Another challenge with growing HPSC thin films epitaxially for devices is the fact that HPSCs must be grown on substrates that are not single crystalline.[62] In perovskite-based devices, the intrinsic perovskite semiconductor is sandwiched between electron- and hole-

6

transporting layers (ETLs and HTLs, respectively). The ETL and HTL are essential to the function of these devices to reduce the recombination of the free charge carriers,[63, 64] as illustrated by the band diagram in Figure 1b.[65] However, the ETL and HTL materials are not perovskites or even not single crystalline, on which surface single-crystal thin films are supposed to be prepared.[66] Although some research groupshave transferred single crystal halogen perovskite films from as-grown substrates to the surface of ETLs, the transfer process has limited the film area., and it is also not suitable for single-crystal films of tens of nanometres thickness.[67, 68] Even with extensive studies, it is still difficult to grow single-crystal $MAPbX_3$ and $CsPbBr_3$ films on either ETL or HTL since most ETL or HTL materials are polycrystalline and their crystal lattices do not match with HPSC thin films.[69, 70] Thus, light-emitting devices based on $CsPbBr_3$ composite are currently restricted to the polycrystalline form,[71] as its HPSC thin films are found to be very difficult to be integrated into devices. The high-quality fabrication of HPSC ultra-thin films on arbitrary substrates is an open challenge currently under active investigation, [72, 73] since single crystal thin films do not naturally grow on arbitrary substrates without proper lattice matching.

Figure 2 shows the general schematic of the epitaxial growth (Figure. 2a, b, c). Epitaxy is generally divided into two major types, homoepitaxy and heteroepitaxy.[74] Materials scientists have exploited many fabrication methods for epitaxial halide perovskite thin films growth, which varies from individual structure, properties and the application conditions of thin films and substrates, as well as the lattice mismatch between them.[75] As a result, to select a proper epitaxial thin film growth technology, researchers should take into account thermodynamics, kinetics, surface energies, materials scalability, samples reproducibility, stability and commercial applications.[76, 77] These typical epitaxial growth methods, such as the vapor-phase epitaxy, liquid-phase epitaxy, molecular-beam and solid-phase epitaxy, as well as other kinds of thin-film fabrication methods, guarantee the quality of single-crystal thin films.[78, 79]

Using epitaxial growth, the flexibility of the device design of perovskite materials is greatly improved, so is the tunability of layer thickness, and also the device performance in regards to electronic properties Below we discuss several epitaxy strategies that have been employed to approach the high-quality HPSC thin films in the following.
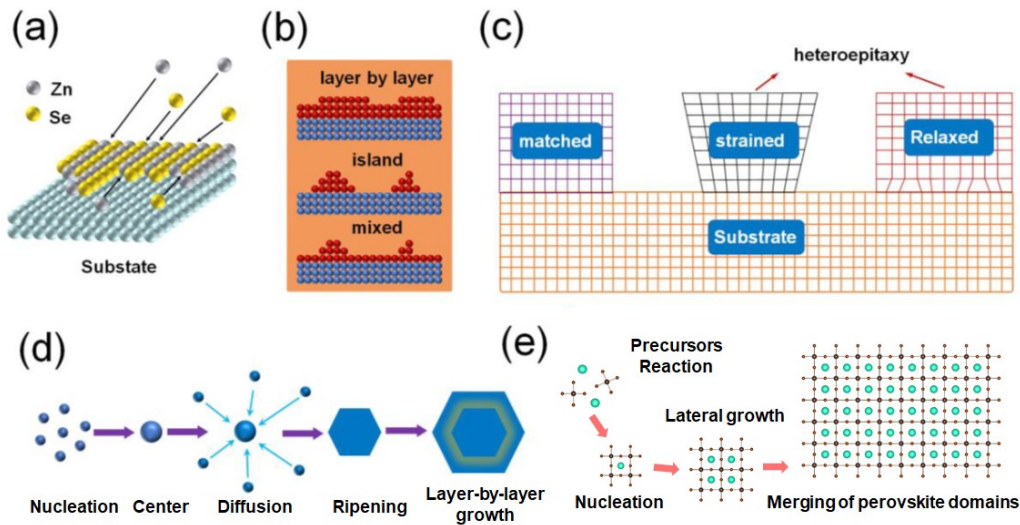
Figure 2. a,b,c) Schematic diagram of the epitaxial film growth on a matching single crystal substrate. d,e) Schematic diagram of the self-assembly of single-crystal slice on a smooth substrate.

2.1.1 **Solution-phase growth on lattice-matched substrates.** To identify lattice-matched substrates for organic-inorganic hybrid HPSC thin films, Chen et al. prepared a series of halide perovskite substrates of $MAPbCl_xBr_{3-x}$ to engineer epitaxial single-crystal α-$FAPbI_3$ thin films (**Figure 3**a).[80] Substrate customization is achieved by tailoring the composition, thereby tuning the lattice parameters until the ideal mismatch is found.The main parameters of a typical example are shown in **Table 1**. The designed lattice mismatch between film and substrate can precisely control the film's strain. The lattice parameter of strain-free (001) α-$FAPbI_3$ and (001) $MAPbCl_xBr_{3-x}$ substrate are 6.35 Å and 5.83-5.95 Å, respectively. α-$FAPbI_3$

film is able to epitaxially grow on the substrates with the Cl$^-$ fraction ranging from 0 (MAPbBr$_3$) to 50% (MAPbCl$_{1.50}$Br$_{1.50}$, lattice parameter of 5.83 Å), where α-FAPbI$_3$ was subjected to the maximum tolerance compressive strain of 2.4% for thermodynamical steady epitaxial growth. Instead of van der Waals interactions, the lattice-mismatch promotes the strong chemical bonds, which constrains the epitaxial lattice to the substrate and restricts the lattice from the phase transition. In addition, the epitaxial film under compressive strain also neutralizes the effect of the internal tensile strain that induced the phase transtion. The two reasons are the key to α-FAPbI3 phase stabilization and subsequent the environmental stability against temperature and pressure variation. The strain promoted the growth and stability of the α-FAPbI$_3$ crystal structure, reduced the bandgap, increased hole mobility enhanced the stability. This conclusion was supported not only by experimental techniques but also by the theoretical calculations, indicating the epitaxial single-crystal perovskite thin film is a promising candidate in photodetector devices. Such strain engineering can be used to enhance device performance. For example, photoconductor structured photodetectors of Au/α-FAPbI$_3$/indium tin oxide with −1.2% strain were reported to exhibit dark current (at −1 V) and photocurrent approximately 15% and 180% greater than those of their strain-free counterparts. These enhancements are attributed to the higher defect density in the strained device and the higher carrier mobility as well as better alignment of valence-band maximum to the Fermi level of the Au electrode in the strained photodetector device

2.1.2 Epitaxial growth on intermediate layers. Besides the efforts made to epitaxial growth of HPSC films to improve the working efficiency, interlayer insertion is introduced as an auxiliary way for the device performance enhancement.[81] MoS$_2$ is fabricated between the hole-transport poly[bis(4-phenyl) (2,4,6-trimethylphenyl)amine] (PTAA) and MAPbI$_3$ film. The addition of MoS$_2$ flakes contributes to not only the perovskite thin films orientation preference, due to the lattice matching between the thin films and interlayer contact surface,

but also the enhancement of stability and photoelectronic properties, such as photovoltaic power conversion efficiency, owing to the improvement of both the thin film crystalline and the interface hole extraction and transfer rate. The spin coating method was used for the interlayer growth.[82]

Antisolvent treatment method, one of the most effective strategies for large-scale and high-quality perovskite film preparation, as been used to crystallize $MAPbI_3$ on MoS_2 interlayers. [83] An antisolvent was used to reduce the solubility of $MAPbI_3$ to facilitate the crystallization, and as a result, the epitaxial perovskite thin films were developed after annealing (process is shown in Figure 3b and the related parameters are summarized in Table 1).[84] It is worth noting that post-treatment of the HPSC thin films can effectively reduce surface traps that lower the efficiency of the devices.[85] Although the lattice symmetries of hexagonal MoS_2 and tetragonal $MAPbI_3$ are different, the surface of MoS_2, which is free of dangling bonds, can accelerate Van der Waals epitaxial growth of $MAPbI_3$ thin film by facilitating atom migration.[86] As a result, the lateral direction grain size growth is accelerated. $MAPbI_3$ thin film epitaxial growth takes place as the interplanar distances of $MAPbI_3$ (008) plane and MoS_2 (110) plane are both 1.58 Å. The lattice mismatch between the film and the substrate is reduced to the minimum (~0%) due to the relation of $d_{(002) MAPbI3} = 4 \times d_{(110) MoS2} = 6.32$ Å. The application of $MAPbI_3$ and MoS_2 heterojunction-based solar cell devices was investigated over a series of different devices with different MoS_2 average grain sizes. A PCE of 20.55%, close to the record efficiency of HPSC thin film solar cells, was reported for the champion device with 500 nm MoS_2 flakes. The carrier transport efficiency facilitated by both MoS_2 modification and $MAPbI_3$ orientation was used to rationalize the enhancement of the properties. Additionally, the time-resolved photoluminescence, external quantum efficiency and other properties also demonstrated the advantage of devices fabricated with MoS_2 flakes.

2.1.3 Exfoliation and transfer of epitaxial films. $MAPbX_3$-based HPSC films have promising outlook in wearable and implantable photovoltaic and electronic devices, thanks to the benefits of the encapsulating and packing techniques, such as poly(dimethylsiloxane) (PDMS) encapsulation.[87-91] However, considering the volatile and vulnerable organic components in the brittle inorganic framework in organic-inorganic hybrid halide perovskites, [92] high flexibility and high performance are not easy to be obtained concurrently. Various approaches to flexible HPSC are designed and adopted, to exfoliate films from hard substrates so that they can be transferred to flexible ones or remain as freestanding films. Lei et al. reported a solution-based lithography-assisted epitaxial-growth-and-transfer method for preparing flexible $MAPbI_3$,[43] whose properties are shown in Table 1. As shown in Figure 3c, the single-crystal perovskite substrates in the growth mould were merged into the $MAPbI_3$-based solution. Small crystals nucleated, filled and grew out of the pattern openings, merged into a continuous thin film. Afterward, the film was lifted and rotated in-plane to break the connection with the substrate. TEM was used to confirm that the crystal lattices of epitaxially grown $MAPbI_3$ films were the same as those of single-crystal $MAPbI_3$ substrate due to the high-quality homoepitaxy. Devices with 2 μm thick $MAPbI_3$ absorber exhibited the highest light absorption. The device current density improved with the thickness of $MAPbI_3$ increasing until 2 μm and impaired with the thickness continuously rising because of the light absorption saturation with the carrier collection efficiency limitation. The fill factor (*FF*) and the open-circuit voltage (V_{OC}) decreased with increasing thickness due to the weaker build-in field in thicker films induced stronger interfacial charge accumulation. The high short-circuit current density (J_{SC}) in $MAPb_{0.5}Sn_{0.5}I_3$ and bandgap-graded $MAPb_{0.5+x}Sn_{0.5-x}I_3$ resulted from the bandgap and the exciton binding energy decreasing when tin was alloyed with lead.Furthermore, each device unit was able to be interconnected by the metallic bridge to form a flexible island-bridge array, reaching the working area of 6.25 cm^2. Neither the

flexibility nor the high performance of the devices is decreased. For example, the bandgap-graded $MAPb_{0.5+x}Sn_{0.5-x}I_3$-based solar cells exhibit an average efficiency of 18.77%.
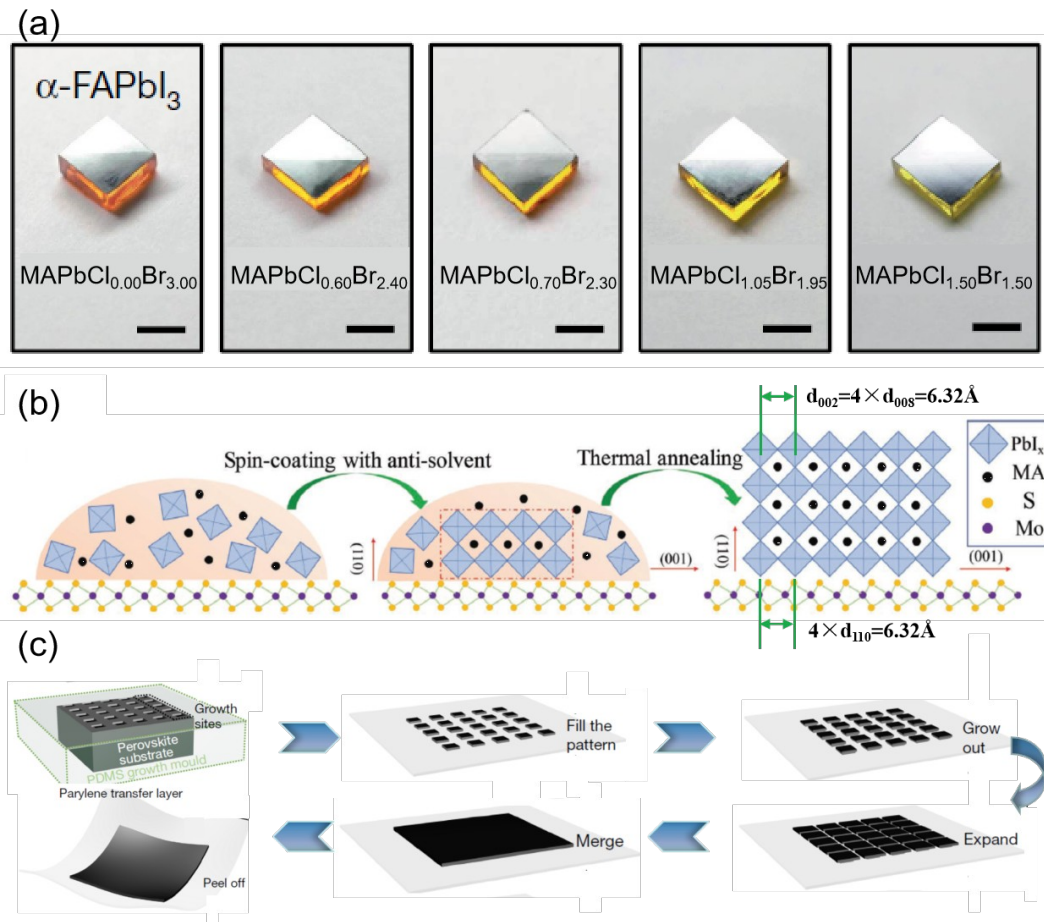
Figure 3. Epitaxial growth of organic-inorganic hybrid HPSC thin films, such as (MA, FA)PbX$_3$. (a) The heterojunction design schematic of α-FAPbI$_3$ grown on a series of MAPbCl$_x$Br$_{3-x}$ (0.00 ≤ x ≤ 1.50) substrates. Reproduced with permission.[80] Copyright 2020, Nature. (b) The MAPbI$_3$ perovskite growth process including spin-coating with anti-solvent, thermal annealing and heteroepitaxy on (110) MoS$_2$ substrate. Reproduced with permission.[18] Copyright 2019, John Wiley and Sons. (c) The fabrication flow diagrams of MAPbI$_3$-based (MAPb$_{0.5+x}$Sn$_{0.5-x}$I$_3$) single-crystal thin film, including solution-based epitaxial growth, expanding, merging and transferring steps. Reproduced with permission.[54] Copyright 2020, Nature.

2.1.4 Epitaxial spin coating method. . To assemble perovskite-based devices, the sandwich structure of ETL/halide perovskite/HTL is typically necessary.[57, 93] As a result, most single-crystalline perovskites grown on non-transport layers, such as SrTiO$_3$ substrates, inevitably suffer from the challenge of exfoliating and transferring, which requires a precise operation.

To avoid the defects produced in this process, the alternative method, the direct fabrication of the perovskite single crystals on transport layers has been utilized.[94] The properties of a typical example are listed in Table 1. A series of (100) CsPbBr$_3$ arrays were in situ grown on cubic phase (100) ZnO ETLs by the spin-coating method. The large lattice mismatch causes CsPbBr$_3$ to form μm-scale single-crystal arrays instead of the large-area continuous films. Although there is more space for the evolution from single-crystal arrays to thin films, the experiment design and method lead the way in the one-step method for single crystal perovskites-based semiconductor compatible devices.[95]

Similar work by Kelso and their coworkers introduced the epitaxial CsPbBr$_3$ spin coating method.[52] The process and the mechanism were analyzed in **Figure 4**a. After the material solution was dropped on the (100) SrTiO$_3$ spinning substrate, the boundary layer and the ordered adlayer formed. Nucleation occurred as the spinning and heating faciliated evaporation of and supersaturation of the solution. The accompanying concentration reduction at the interface of solid and liquid caused the concentration gradient which results in the diffusion layer component of molecular or ion. The structure of spin-coated CsPbBr$_3$ was illustrated by the interface model, which is shown in Figure 4b. A +5.57% lattice mismatch between CsPbBr$_3$ (100) [011] ∥ SrTiO$_3$ (100) [001] was achieved by 45° in-plane rotation of CsPbBr$_3$. The lattice mismatch is relatively large (>4%) so that the continuous film area is limited. The corresponding X-ray pole characterization also confirmed the single-crystal out-of-plane and in-plane orientations relative to SrTiO$_3$ substrates. SEM image of (100) SrTiO$_3$ substrate grown CsPhBr$_3$ is shown in Figure 4c. The diamond-like island of CsPbBr$_3$ has the potential to become dense films with more depositing times or additives to adjust its chemical interfacial energy.[96, 97] This simple and economical spin coating method is should inspire further development of epitaxial halide perovskite thin films.

2.1.5 Vapor-phase expitaxy.

Inorganic perovskites have lower solubility and more complex phase diagram, resulting in a more challenged solution growth. Vapor-phase epitaxial (VPE) growth is a powerful technique, which has advantages in controlling morphology, reducing defects and monolithic device integration.For example, $CsPbBr_3$ have been deposited via VPE by adjusting the lattice mismatch by calculating lattice constants. Figure 4d shows a representative chemical vapor deposition tube-in-tube setup, in which $CsPbBr_3$ ingots are used as the source for depositing epitaxial films on a $SrTiO_3$ (100) substrate. Different temperatures and operation times produced different $CsPbBr_3$ morphologies. Compared to discrete $CsPbBr_3$ nanoplates, continuous $CsPbBr_3$ films required higher temperature to promote the diffusion of adatoms and accelerate the preferred epitaxial crystallite nucleation. $CsPbBr_3$ materials were heteroepitaxially fabricated on multifunctional oxide perovskite $SrTiO_3$ (100) substrate in vapor-phase epitaxial growth method.[98] Although $SrTiO_3$ and $CsPbBr_3$ share the same cubic crystal structure, the lattice constants of $SrTiO_3$ (3.91 Å) and $CsPbBr_3$ (5.83 Å) have large mismatch. Serendipitously, however, a low mismatch of 0.47% occurs between two unit cells of $CsPbBr_3$ and three-unit cells of $SrTiO_3$, where 150% times the lattice constant of $SrTiO_3$ conforms to 100% that of $CsPbBr_3$ in both $CsPbBr_3$ (100) [100] ∥ $SrTiO_3$ (100) [100] and $CsPbBr_3$ (100) [010] ∥ $SrTiO_3$ (100) [010] directions. As shown in Figure 4e, the overlap area illustrated by the light yellow consists of the unit cells of 2×2 $CsPbBr_3$ (100) or 3×3 $SrTiO_3$ (100). Because of the Volmer-Weber island formation heteroepitaxial growth mode, $CsPbBr_3$ forms rectangular islands in all sizes where the large surface energy and the $SrTiO_3$ surface wetting layer absence may dominate the morphology. The minority thick nanoplates exhibited concave surfaces, following the layer-by-layer inverted wedding cake homoepitaxial growth mechanism. Here, the nucleation of the new atomic layers occurred at the edge, fabricating inward and then being trapped in virtue of the interlayer mass transport.
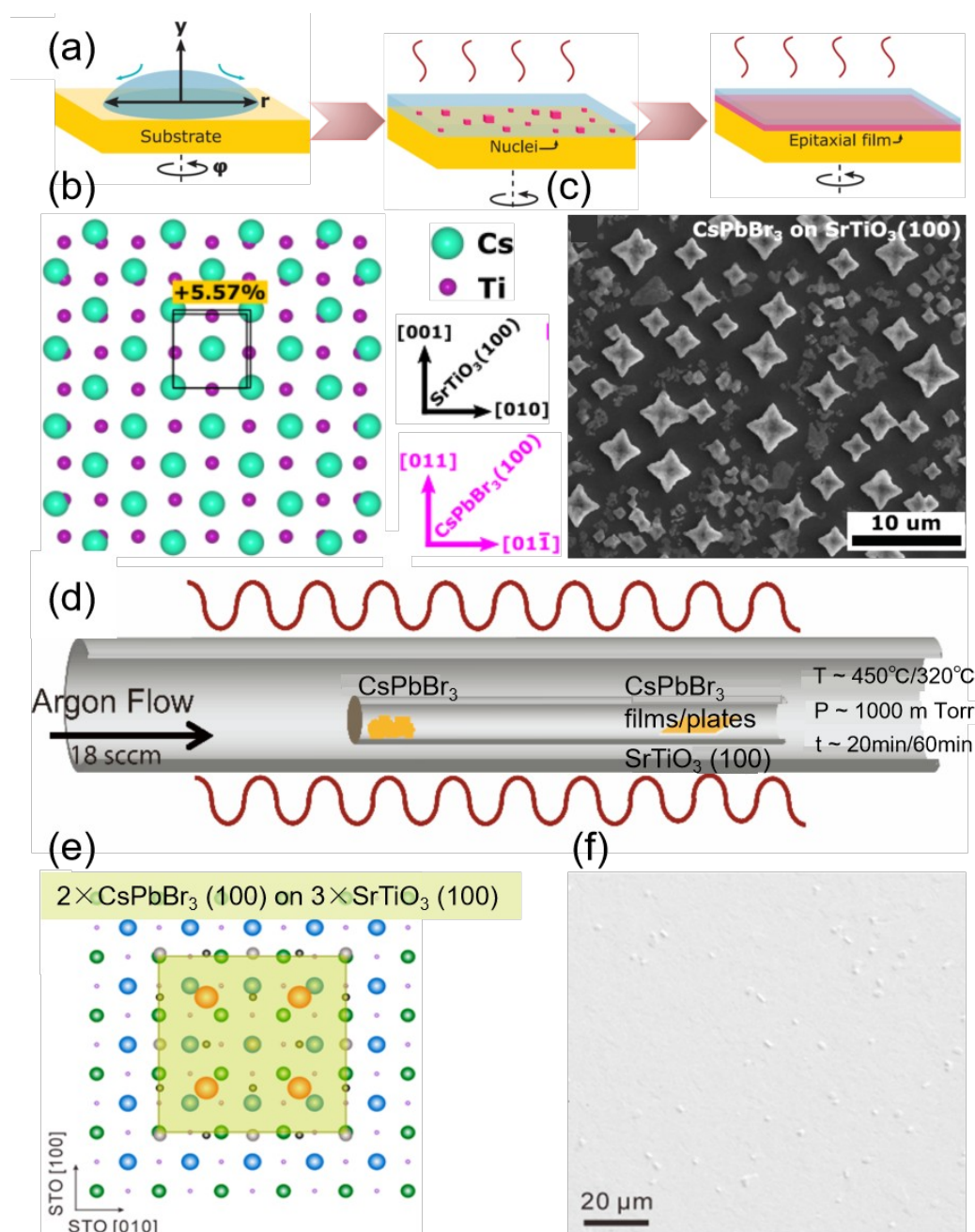
Figure 4. Epitaxial growth of all-inorganic HPSC CsPbBr$_3$ thin films. (a) The diagram of spin coating process and mechanism of epitaxial thin films fabrication. (b) The interface model of CsPbBr$_3$ (100) [011] and SrTiO$_3$ (100) [001], showing the lattice mismatch of +5.57%. The green spheres indicate Cs atoms and the purple spheres represent Ti atoms. (c) The SEM data of CsPbBr$_3$ on SrTiO$_3$ (100) substrate. Reproduced with permission.[60] Copyright 2019, American Association for the Advancement of Science. (d) The tube-in-tube vapor phase equipment for CsPbBr$_3$ single-crystal thin films and nanoplates epitaxial growth on SrTiO$_3$ substrates. (e) The structure illustration of incommensurate lattice match structure between 2 unit cells of CsPbBr$_3$ (100) and 3 unit cells of SrTiO$_3$ (100). (f) The SEM image of the CsPbBr$_3$ single-crystal thin films smooth surface with few concave textures. Reproduced with permission.[98] Copyright 2017, American Chemical Society, from the link https://pubs.acs.org/doi/abs/10.1021/jacs.7b07506, and further permissions related to the material excerpted should be directed to the ACS.

Higher reaction temperature and shorter process time were needed to obtain the continuous CsPbBr$_3$ thin films. Randomly irregular nanostructures formation was avoided due to the broken of Volmer-Weber mode that accelerates the adatoms diffusion and the increase of nucleation density. The smooth surface of large-scale CsPbBr$_3$ single crystal thin film is shown in Figure 4f, and the small concave textures were consistent with the layer-by-layer homoepitaxial growth mode during the CsPbBr$_3$ thick nanoplates growth. The device was configured as Au/CsPbBr$_3$/Au. 10^{12} cm^{-3} defect density, 10^4 cm s^{-1} surface recombination velocity and the slow charge carrier recombination rate were observed. The method of facile vapor-phase heteroepitaxial halide single-crystal thin films growth on perovskite oxide substrates reported in this work is typical and possesses the applicable universality to some extent. As a result, we have reasonable grounds to believe that more and more promising heteroepitaxial growth involved halide and oxide perovskites would be achieved in the coming future in optoelectronic devices.[98]

2.2. Lateral growth of HPSC films

Unlike epitaxial growth, which requires lattice-matched growth on crystlaline substrates, HPSCs can be grown on arbitrary substrates using a second class of HPSC fabrication known as lateral growth. Lateral growth of HPSC films usually occurs through nucleation at many different sites on the substrate, where each of the newly grown nuclei grow laterally in parallel. Although the film may become polycrystalline over a larger area, there can be regions of micro-, milli- or even centimeter-scale single-crystal films stemming from growth on one nucleus. Owing to the relatively loose substrate selection rules of HPSC films lateral growth, it is favorable to the development of various on-chip fabricate perovskite applications, including flexible devices making use of HPSC film/PET, perovskite solar cells

in the structure of HPSC film/ITO, electronic devices with HPSC film/Si, and optical devices applying HPSC film/quartz structure.

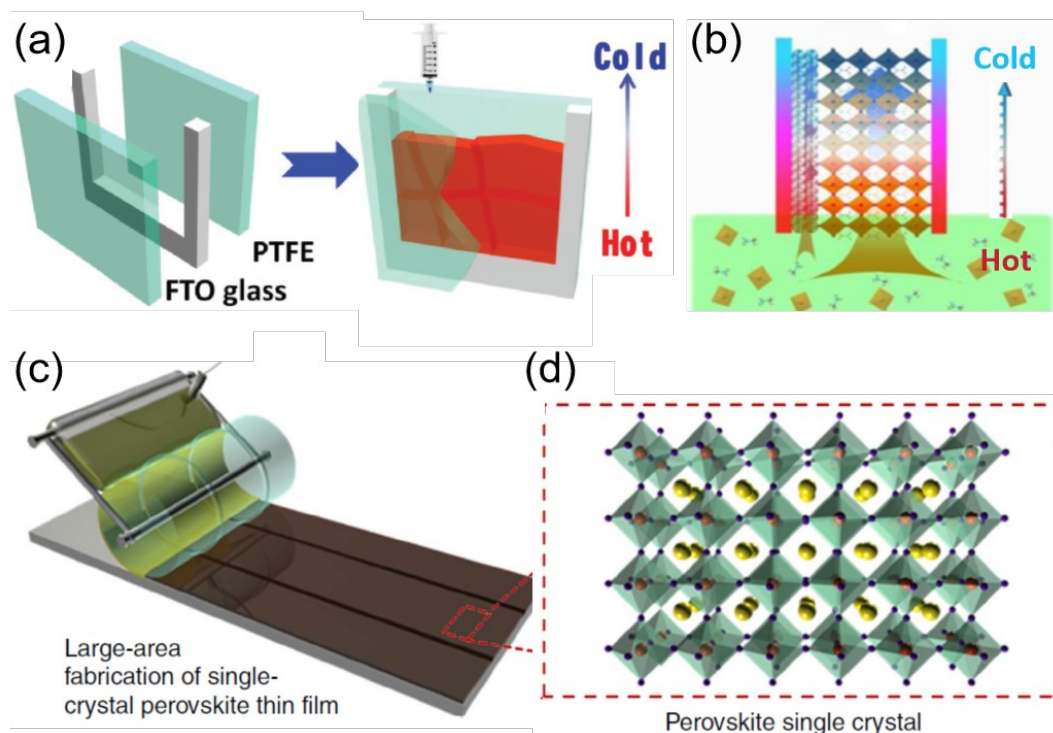**2.2.1 Geometrically-restricted lateral growth.**

Seeking to work around the strict lattice matching required by epitaxial growth on horizontal substrates, scientists have developed alternate methods for HPSC film growth based on confining the growth of single-crystal thin films in the vertical direction between two parallel substrates, thereby promoting lateral growth of single crystals.[99, 89] The specific details are introduced in the corresponding examples and shown in Table 1.[99, 100] For example, the space-limited inverse temperature crystallization method was employed to fabricate $MAPbBr_3$ crystal film between fluorine-doped tin oxide (FTO) glass and polytetrafluoroethylene (PTFE) substrates, where the inserted U-shape PTFE substrates regulate $MAPbBr_3$ film thickness (**Figure 5**a).[89] Crystal growth using this method is initially disordered. Subsequently, the (100) crystallographic direction dominates, resulting in large (100)-oriented crystals. This result can be explained by the (100) exposed face obtained in the XRD pattern of $MAPbBr_3$ powder and crystal film. With the temperature gradient, the injected $MAPbBr_3$ precursor solution was synthesized *in situ* to produce the films with areas as large as 120 cm^2. Narrowband photodetectors fabricated using the resulting materials offer broad linear response over incident light power densities from 10^{-4} to 10^2 mW cm^{-2} with wavelength selectivity of 61.3 dB, 3 dB cutoff frequency of ≈ 110 kHz, and high narrow response under the low bias of -1 V. Similarly, Zhao et al. demonstrated the fabrication of $MAPbI_3$ perovskite solar cells (Figure 5b) by dipping two parallel FTO/TiO_2 substrates vertically into a heated $MAPbI_3$ precursor solution.[89] Due to capillary pressure and the temperature gradient, solutions were wicked in between the substrates and subsequently reacted to form single-crystalline $MAPbI_3$ films. The thickness of each film was controlled by the gap between the two substrates, produced by a 50-200 μm thick Teflon spacer. The [001]

vertical direction of MAPbI$_3$ dominated during the growth process. The relevant solar cell devices were fabricated a FTO/TiO$_2$/MAPbI$_3$/Spiro-OmeTAD/Ag architecture, where TiO$_2$ and Spiro-OmeTAD served as the ETL and HTL, respectively. The charge extraction efficiency at TiO$_2$/MAPbI$_3$ interface was high, the MAPbI$_3$ single crystal thin films' optic band gap was small and the carrier lifetime was long. Devices were measured to have maximum short circuit current density J_{SC} of 24.40 mA cm^{-2}. The on-substrate fabrication method was also used by Chen et al. .[100] to grow MAPbBr$_3$ MAPbI$_3$, MAPbCl$_3$ thin films that can exhibit visual inspection thickness-dependent colors. Various substrates, such as the silicon, flexible polyethylene terephthalate (PET), mica, ITO and FTO, can be applied without lattice matching to the thin films. Fabrication was realized according to top-seeded solution-growth, with the temperature gradient inducing sufficient convection in the solution. The thin film device was observed to have trap density n$_{trap}$ ~ 4.8 × 10^{10} cm^{-3}, carrier mobility μ ~15.7 cm^2 V^{-1} s^{-1} and carrier lifetime τ$_r$ ~84 μs.[100]

A similar HPSC thin film fabrication process of cast capping was employed to grow MAPbBr$_3$ and applied to LED devices. The single crystal was formed after casting perovskite precursor solution on a ITO-patterned glass substrate and was then capped by another ITO-coated substrate. A LED device based on ITO/MAPbBr$_3$/ITO sandwich structure emitted pure green luminescence with a full width at half a maximum of 20 nm at operating voltages as low as 2 V. The electroluminescence blinking behavior of this device may provide insight into the recombination processes that depend on carrier traps and defects in HPSC light-emitting applications. [101]

To form large-scale HPSC MAPbI$_3$ thin films, a fabrication mould can be applied, property details shown in Table 1.[102] The patterned rolling mould is implemented to roll-print the perovskite ink solution onto substrates, during which the solvent evaporates accompanying the feeding solution crystallization by heating the substrate to form the

unidirectional lateral growth within the geometrical confinement. The flexible poly(dimethylsiloxane) (PDMS) mould was prepared with periodical channels and narrow spaces to wrap on a metal roller. When it rolled on SiO_2 substrate, the $MAPbI_3$ precursor solution mounted in the ink supplier was printed (Figure 5c) in the tetragonal crystal structure (Figure 5d). The seed crystals grew initially along the [110] direction in the instant crystallization process. Misaligned growth was prevented by lateral geometrical confinemen,t and the growth on nuclei only occured in one open direction along the substrate until one crystal dominated the channel space. Vertical growth was restricted by kinetic control as well as geometrical confinement. Finally, the single-crystal structure of the film is confirmed by XRD scan at the fixed 2θ angle of (002) plane, where the tetragonal perovskite four-fold symmetry is proved via the four sharp peaks. It indicates that the [001] direction finally dominates in film laterally growing in the channels of the mould. The area of the patterned thin film can reach 3×3 inches. A single-crystal $MAPbI_3$ model device was fabricated with 200 nm thickness and two 100-µm-gap Au electrodes deposited on the surface. A hole mobility of 45.64 cm^2 $V^{-1}s^{-1}$ was obtained under 3 V, reaching the bulk single crystal perovskite level. The $MAPbI_3$ based lateral solar cells were characterized in a Au/$MAPbI_3$/PCBM/Ag configuration . The short-circuit current density was 18.33 mA cm^{-2}, the open-circuit voltage was 0.801 V, the fill factor was 0.329 and the best active-area PCE was 4.83%, confirming the high performance relative to other lateral perovskite solar cells Vertically restricted lateral growth methods pave a way for the further exploration of high-performance single-crystal thin films, different from horizontal epitaxial fabrication.

Figure 5. Solution-based geometrically-restriction lateral growth. (a) The sandwich structure for $MAPbBr_3$ crystal films growth under the temperature gradient, the thickness being controlled by that of U-style PTFE thin membrane. Reproduced with permission.[44] Copyright 2017, John Wiley and Sons. (b) The schematic of single-crystalline $MAPbI_3$ growth on vertical FTO/TiO_2 and glass substrates with the temperature gradient. Reproduced with permission.[89] Copyright 2017, Elsevier on behalf of Science in China Press (China). (c) The schematic of geometrically confined lateral crystal growth. The single-crystal thin film is roller-printed by the roller mould with the thin film solution ink supplier, resulting in rapid crystal growth in the rolling direction. (d) The printed single-crystal $MAPbI_3$ perovskite thin films crystal structure, the yellow sphere denoting the $CH_3NH_3^+$, red sphere being Pb^{2+}, and violet sphere referring to I^-. Reproduced under terms of the CC-BY license.[102] Copyright 2017, Lynn Lee et al., published by [Springer Nature].

2.2.2 Solution-phase lateral growth with external stimuli

Preparing the hybrid perovskite crystals in solution is one of the widely used ways to grow single crystals,[103, 104] among which the external stimulus of adjusting the solution saturation plays an important role. To achieve single-crystal thin films, a specially designed solution-based method was exploited using cavitation-triggered asymmetrical crystallization (CTAC), in which a short ultrasonic pulse ($\approx$ 1 s) is introduced to promote $MAPbBr_3$ nucleation (Ultrasonic stimulation in Table 1).[105] The prepared $MAPbBr_3$ semitransparent

homogeneous films are free of grain boundaries (**Figure 6**a). To fabricate the films, equimolar MABr and $PbBr_2$ perovskite precursor solution was sealed in a dish with a 0.5 mm diameter hole, which was put into a larger dish with dichloromethane antisolvent. A short ultrasonic pulse was actuated in the ultrasonic bath when the perovskite solution reached a low supersaturation in order to provide the energy for heterogeneous nucleation by means of rapid local cooling. The local pressure and accumulating energy in a cavitation process were increased. Thus the cavitation bubbles asymmetric around the substrate, resulting in the initial stage preferential lateral crystallization through the jet shooting to the substrate (Figure 6b and 6c).[105] Varying the precursor concentrations was used to tune film thicknesses from one to several tens of micrometers. High-resolution X-ray diffraction (XRD) further confirmed a fourfold symmetry in (110) diffraction, explaining the film's (001)-oriented cubic symmetry in twin-free single crystals. Many substrates can be used to anchor the perovskite films in this method, e.g., FTO-coated glass. A photovoltaic device based on a glass/FTO/TiO_2/$MAPbBr_3$/Au structure was fabricated, with $MAPbBr_3$ thin film as the light absorber layer and TiO_2 (or Au) film as the ETL (or HTL). Optoelectronic devices based on $MAPbBr_3$ HPSC films exhibited stability advantages over analagous polycrystalline devices, since grain boundaries served as moisture infiltration and corrosion sites in polycrystalline films.

Lateral growth with external stimuli is also used to grow freestanding single-crystal thin films, for example, $CsPbBr_3$ thin films with lateral size as large as nearly centimeters were reported.[106] In order to achieve highly anisotropic single-crystal thin films, precursor concentration, reaction temperature, and surfactant are the rival parameters. The growth strategy combined with the chemical vapor deposition and chemical solution process is called external stimulied lateral growth, with the typical example details in Table 1. As shown in Figure 6d, the glass dish containing dissolved $PbBr_2$, CsBr and the acid was placed in the sealed bottle with the mixed anti-solvents . The freestanding and flexible thin-film shown in

Figure 6e was on the scale of several millimeters, displaying transparent yellowish color. Confirmed by both experimental data and first principles density functional theory calculations, the ligand of the surfactant plays an important role in effectively modifying the film surface energy, resulting in the large ratio between the film lateral size and the thickness. Surfactant content increase thickens the vertical size and thins the lateral size of the films. The surface energy and temperature influence the $CsPbBr_3$ single-crystal film growth rate, according to the crystal growth kinetics **Equation 3**:

$$\psi = A \exp\left[-\left(E_A - E_s\right)/\left(k_B T\right)\right] \qquad (3)$$

Where ψ denotes the growth rate, E_A is the crystal growth activation energy and E_S is surface free energy. The k_B is the Boltzmann constant and T is the reaction temperature. (110) orientation in $CsPbBr_3$ HPSC thin film is confirmed by the data analysis of XRD, electron backscatter diffraction (EBSD) and high-resolution transmission electron microscope (HRTEM). The film is with a 2.31 eV bandgap, corresponding to the film's uniform bright green luminescence. All of the films' uniform optical properties, high crystallinity and bound exciton in vertical direction contribute to the excellent photoluminescence. The carrier mobility ranged from 7 to 45 cm^2 V^{-1} s^{-1} and the trap density is from 5×10^{10} to 5×10^{12} cm^{-3} at the different thickness locations on the same $CsPbBr_3$ HPSC thin film. Analyzed from the data, the photoluminescence lifetime increased while the trap density decreased with the film thickness increasing. The uniform optical property of the film is demonstrated by the tight distribution of photoluminescence lifetime at different regions.[106] The large-scale $CsPbBr_3$ single-crystal thin films have potential in high-performance photoelectric applications.

As another example of external stimulied lateral growth, single-crystal $MAPbBr_3$ microplatelets were grown on ITO/glass substrates placed in $MAPbBr_3$/Dimethylformamide (DMF) precursor solution in a Teflon beaker, which was sealed in a glass beaker containing

Dichloromethane (DCM) for 24 hours at room temperature.[106] A simple ITO/MAPbBr$_3$/Au LED device was fabricated without any ETL or HTL, Here, ion migration was used to form the p-i-n junction. The deve emitted 2.3 eV photons under 1.8 V for 54 hours at ~5000 cd m^{-2} without degradation. Moreover, whispering-gallery-mode cavities and exciton-exciton interaction have been demonstrated in the same device, highlighting the potential of electrically driven HPSC laser diodes. [107]
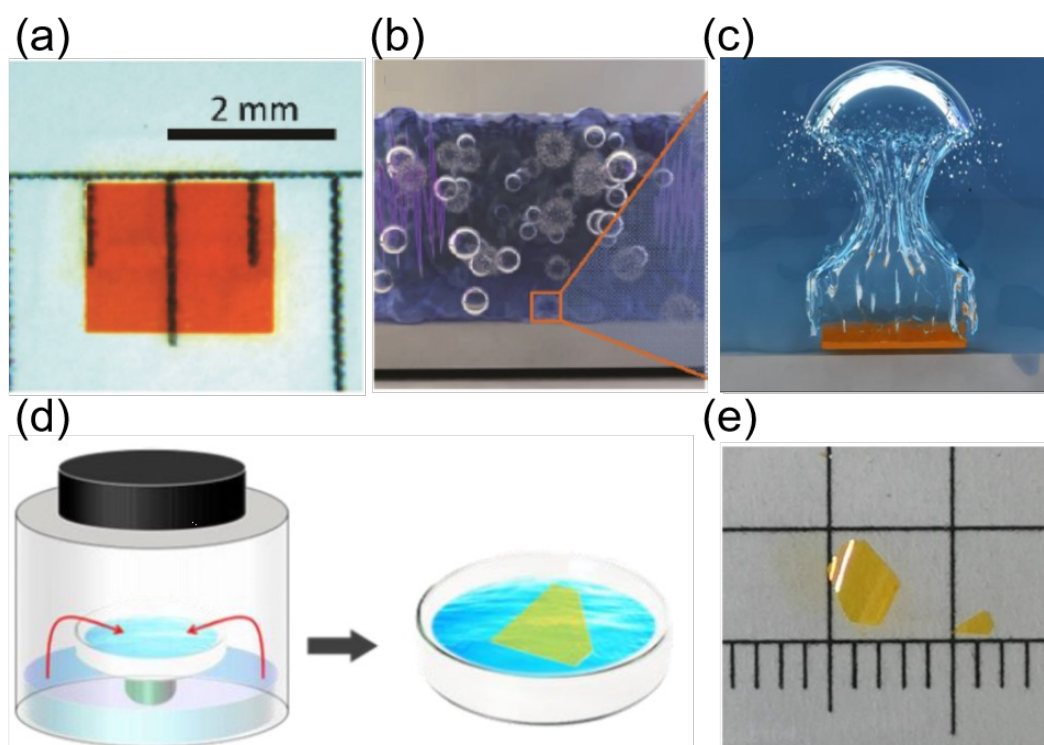
Figure 6. Solution-based external stimulus lateral growth. (a) The image of the MAPbBr$_3$ single crystal thin film, demonstrating the large scale of the film. (b) The film fabrication process. The collapse of the cavitation bubble near the substrate, which is asymmetric and causes a high-speed jet toward the substrate, resulting in the initial stage preferential lateral crystallization origin. (c) Zoom image of the bubble acting on the substrate and film. Reproduced with permission.[105] Copyright 2016, John Wiley and Sons. (d) The modified antisolvent diffusion process for CsPbBr$_3$ single-crystal film synthesis in solution. (e) The photography of yellowish CsPbBr$_3$ single-crystal film in solution, showing the transparency and flexibility. Reproduced with permission.[106] Copyright 2020, John Wiley and Sons.

Table 1. Summary of representative epitaxial and oriented HPSC thin films

Material	Method	Substrate	Thin film status	Lateral size	Thickness [μm]	$\mu^{c)}$ [cm^2 s^{-1} v^{-1}]	Lifetime [ns]	$N_{trap}^{d)}$ [×10^{11} cm^{-3}]	Device	Ref.
Epitaxial methods										
α-FAPbI$_3$	Solution-phase	MAPbCl$_x$Br$_{3-x}$	Single crystal	>12 μm × 12 μm	0.50	~100	-	5.30	Photodetector	[80]
MAPbI$_3$	Intermed. layer	MoS$_2$ flakes	Preferred orientation	90 nm; 250 nm; 500 nm	0.40	-	22.43	-	Photovoltaic	[22]
MAPbI$_3$ MAPb$_{0.5}$Sn$_{0.5}$I$_3$	Exfoliation	MAPbI$_3$	Single crystal	5.50 × 5.50 cm	0.06-100	~40	~600	2.20	Photodetector	[54]
CsPbBr$_3$	Spin Coating	c-ZnO	Single crystal	10 × 3 μm	-	-	3.64; 20.90	-	-	[94]
CsPbBr$_3$	Spin Coating	Au/Si	Epitaxial	<10 μm	-	-	-	-	-	[60]
CsPbBr$_3$	Vapor-phase	SrTiO$_3$	Single crystal	5 × 10 mm	1-7	518	10	15	Photodetector	[98]
Lateral growth methods										
MAPbI$_3$	Geometric restriction	FTO/TiO$_2$	Single crystal	>several hundred μm	50-200	-	206	-	Photovoltaic	[89]
MAPbBr$_3$	Geometric restriction	FTO	Single crystal	Area ~120 cm^2	≤1	40.7		0.88	Photodetector	[99]
MAPbBr$_3$ MAPbI$_3$ MAPbCl$_3$	Geometric restriction	PET/glass	Single crystal	Up to mm	≤1	15.7	84000	0.48	-	[100]
MAPbBr$_3$	Geometric restriction	ITO-patterned glass	single crystal	-	-	(20 nm fwhm)	(2 V operating)	-	LED	[101]
MAPbI$_3$	Geometric restriction	SiO$_2$	Single crystal	30 × 77.20 mm	0.02-1	45.64	-	-	Photovoltaic	[102]
MAPbBr$_3$	External stimulus	Si; ITO-coated glass; FTO-coated glass; Sputter-coated metal	Single crystal	Area ~0.20 cm^2	1-90	-	-	~1	Photovoltaic	[105]
CsPbBr$_3$	External stimulus	Freestanding	Single crystal	~1 cm	0.09-0.85	7 to 45	12.60-21	0.50-50	-	[106]
MAPbBr$_3$	External stimulus	ITO/glass	Single crystal	20-100 μm	10	(emiting 2.3 eV photons)	(turn-on voltage of 1.8 V)		LED	[107]

$^{a)}$Epitax., Epitaxial Method; $^{b)}$Later., Lateral Method; $^{c)}\mu$, carrier mobility; $^{d)}N_{trap}$ for trap density.

3. Conclusion and Perspective

HPSC thin films occupy an important position in optoelectronic applications owing to their

remarkable properties of tunable bandgap, long carrier diffusion length, low recombination

rates. Herein, various remarkable works related to the growth methods, materials properties and device applications of HPSC thin films are reviewed. Several typical growth methods are introduced, providing examples of the fabrication of halide perovskite thin films targeted to various goal-oriented characteristics and the specific applications. Furthermore, this review has summarized the recent advancements of properties and applications of photovoltaic devices, photodetectors and light-emitting devices. Although these devices exhibit not only high stability against various degradation factors but also excellent properties. Research on HPSCs is still in its early stages-, particularly, with the concerns about the extreme recombination at the surface of the single crystals. We highlight the challenges that need to be overcome to realize high performance HPSC devices and provide outlook on the future development of these unique materials.

(1) **The extreme recombination** in HPSC thin films or at the surface of the single crystals limits their otherwise excellent photovoltaic performance. More research is needed to understand the in-depth mechanism and then investigated to reduce surface recombination rates. Compared with bulk perovskite polycrystalline crystals, HPSCs and their thin films are affected more by non-radiative recombination induced by surface defects or traps that decrease the carrier mobilities. Therefore, to fully exploit HPSC thin films and enhance their properties in photovoltaic devices, pertinent strategies to understand and control surface defects are urgently needed. The optimization of HPSC quality improvement can include optimizing growth processes and surface passivation techniques to minimize defects. These approaches may include fine or automated control over reaction conditions (e.g., temperature profiles), solvent engineering, [25] post-treatment of thin films, [85] the use of additives during growth, and engineering bandgaps in alloys or heterostructures.[108] Although some research has been performed in these areas, new routes to reducing recombination are waiting to be found.

(2) **Interface engineering** will be another indispensable strategy to unlock the potential optoelectronic performance of the HPCS thin films based devices. To reduce the adverse impact of the lattice strain that exists at perovskite/substrate interfaces due to lattice mismatching, such as the interfacial recombination and electric contact problems, the use of intermediate or buffer layer employment should continue to be employed. More specifically, new interlayer materials and their combinations with substrates should be explored. In addition, issues between other interfaces, such as the perovskite/charge layer and charge/substrate layer should also be investigated more comprehensively.

(3) **HPSC thin-film dimensions** affect properties such as flexibility and high-density integration, which are critical parameters for emerging applications such as wearable electronics. Thus, it is a priority to overcome the challenge of preparing high-quality large-scale 2-dimensional thin films that require large in-plane lateral length or width and small thickness of less than 100 nm along the out-of-plane longitudinal height

(4) **Preparation of HPSCs on compatible ETL or HTL surfaces** is essential for fabricating ultra-thin ETL/perovskite/HTL devices, and the design of new device architectures with advanced properties are needed. Most transfer methods irreversibly damage the films, so it is important to investigate alternate methods, such as the one-step growth of thin films on targeted substrates or even with patterned electrodes, with more compacted attachment and fewer defects. $MAPbI_3$-based devices would benefit from these methods due to the current absence of electron transport layer and hole transport layers for single-crystal thin films for this material.

(5) **Heterojunctions in HSPC devices.** A broader array of HPSC devices could be realized if methods to dope HPSCs and form heterojunctions of such materials could be developed. For example, P-I-N single crystal diodes could be promising based on ETL/perovskite/HTL devices, where P-type semiconductors substitutes for the current ETLs

and N-type semiconductors take the role of the HTLs. Furthermore, fabrication of the PN junctions by directly doping N-type and P-type perovskite single crystal thin film semiconductors would a formative milestone, given that the entire Si-based semiconductor industry is based on fabrication of heterojunctions via doping .[109]

(6) **Improvement in PCE performance** is always one of the most decisive criteria for the state of the art devices. Lowering defect densities and higher carrier mobilities are critical for making progress in this regard. Improvements in growth processing methods will be necessary for achieving these device performance gains, with the goal of exceeding the certified PCE of the commercial silicon solar cells currently in service. Further investigation into coupling of optoelectronic, ferroelectric, and piezoelectric characteristics with mechanical flexibility properties will be of particular value the thin film applications.[110]

(7) **Expanding applications**. In addition to currently investigated optoelectric devices, expanding HPSC film applications to data storage, energy harvesters, catalysis, etc. is a necessity and will be achieved by leveraging the unique ferroelectric properties of HPSCs and their other unique properties. Moreover, multi-functional devices, e.g., those that combine energy generation, management, and storage may increase the application of HPSC materials. Connecting the energy management devices, such as the capacitors, with the photovoltaic cells (generation) as well as other optoelectronics can spur high energy conservation and efficiency.

(8) **Stability improvements**, including thin film robustness, temperature stability and chemical durability, are required for further development of~~industrial~~ HPSC applications. The phase or crystal orientation stability of $MAPbX_3$ has been found to significantly vary with changes in ambient temperature.[111] Compositional engineering of HPSC thin films is required to improve the stability of MA^+ and other perovskites.[38, 108] Adding rigid π-conjugated organic ligands has been demonstrated to stabilize the movement of the ions and prevent the chemical

bonds from easily breaking. Further research is required to develop a wider range of approaches for specificallystabilizing HPSC films.[112]

(9) **Coupling experimental research along with modeling and simulation.** HPSC films will ideally allow perovskite-based devices to approach theoretical limits, which is the goal of most application-oriented research. These goals can be achieved, and the limits can potentially be exceeded, by coupling experimental campaigns to modeling and simulations, e.g., by elucidating epitaxial growth mechanisms, refining design rules for lattice mismatch, and investigating fundamental devices physics. Machine learning [113-115] and high-throughput physical modeling of perovskites [116] can also be combined with traditional and automated experimentation to guide and accelerate the discovery of new routes to synthesizing HPSC thin films, new HPSC materials, and increase understanding of structure-function relationships in these materials. [117-121]

(10) **Industrial scale-up** is another goal for HPSC thin films to achieve during strategies development and challenges overcoming. In this process, many factors should be considered, including the feasibility of high-quality volume production and high product percent of pass. To reduce cost and increase sustainability, fabrication processes with fewer steps, less complex workflows, and mild growth conditions should be developed.

(11) **Development of sustainable materials**. With the further development of HPSC thin film-based devices, the composition of HPSCs will become a more critical concern. The development of perovskites free of lead and other toxic ions will be critical for widespread application of HPSC-based materials. In particular, techniques developed for growing, stabilizing, and treating HPSCs will need to be extended to alternate and more complex perovskite materials, such as double perovskites. [122]

Despite the challenges presented by HPSCs, researchers are forging ahead on the development of these promising materials. While the growth of perovskite single crystals with

such anisotropic and extended dimensions may have seemed unattainable in the past, persistent research has lead to substantial progress, increased understanding, and serendipitous discoveries. We hope that the achievements reviewed here and the future perspective provided inspires more comprehensive and extended studies. Given the breathtaking progress in perovskite research, breakthroughs in HPSC thin film research and applications are on the horizon.

References

[1] W. Deng, Y. Lv, X. Zhang, X. Fang, B. Lu, Z. Lu, J. Jie, *Mater. Today* **2020**, *40*, 82.

[2] S. Kwon, J. Kim, G. Kim, K. Yu, Y. R. Jo, B. J. Kim, J. Kim, H. Kang, B. Park, K. Lee, *Adv. Mater.* **2015**, *27*, 6870.

[3] C. Yue, J. Li, L. Lin, *Front. Mech. Eng.* **2017**, *12*, 459.

[4] S. Han, S. Ji, I. Kang, S. C. Kim, C. You, *Opt. Commun.* **2019**, *430*, 83.

[5] U. Starke, S. Sloboshanin, F. Tautz, A. Seubert, J. Schaefer, *PHYS STATUS SOLIDI A* **2000**, *177*, 5.

[6] K. Kim, M. Hua, D. Liu, J. Kim, K. J. Chen, Z. Ma, *Nano Energy* **2018**, *43*, 259.

[7] P. Dutta, M. Rathi, D. Khatiwada, S. Sun, Y. Yao, B. Yu, S. Reed, M. Kacharia, J. Martinez, A. Litvinchuk, Energy Environ. Sci. **2019**, *12*, 756.

[8] D. Cao, B. Wang, D. Lu, X. Zhou, X. Ma, *Sci. Rep.* **2020**, *10*, 1.

[9] D. S. Tsvetkov, M. O. Mazurin, V. V. Sereda, I. L. Ivanov, D. A. Malyshkin, A. Y. Zuev, *J. Phys. Chem. C* **2020**, *124*, 4252.

[10] A. Pan, Y. Li, Y. Wu, K. Yan, M. J. Jurow, Y. Liu, L. He, *Mater. Chem. Front.* **2019**, *3*, 414.

[11] L. Qiu, S. He, L. K. Ono, S. Liu, Y. Qi, *ACS Energy Lett.* **2019**, *4*, 2147.

[12] A. K. Jena, A. Kulkarni, T. Miyasaka, *Chem. Rev.* **2019**, *119*, 3036.

[13] W. A. Dunlap-Shohl, Y. Zhou, N. P. Padture, D. B. Mitzi, *Chem. Rev.* **2018**, *119*, 3193.

[14] Z. Shi, A. H. Jayatissa, *Materials* **2018**, *11*, 729.

[15] J. Huang, Y. Yuan, Y. Shao, Y. Yan, *Nat. Rev. Mater.* **2017**, *2*, 1.

[16] Y. Lei, Y. Chen, S. Xu, *Matter* **2021**, *4*, 2266.

[17] M. Sampson, J. Park, R. D. Schaller, M. Chan, A. Martinson, *J. Mater. Chem. A* **2017**, *5*, 3578.

[18] M. E. Laamari, A. Cheknane, A. Benghia, H. S. Hilal, *Sol Energy* **2019**, *182*, 9.

[19] A. Kojima, K. Teshima, Y. Shirai, T. Miyasaka, *J. Am. Chem. Soc.* **2009**, *131*, 6050.

[20] W. Yu, F. Li, L. Yu, M. R. Niazi, Y. Zou, D. Corzo, A. Basu, C. Ma, S. Dey, M. L. Tietze, *Nat. Commun.* **2018**, *9*, 1.

[21] T. Matsushima, M. R. Leyden, T. Fujihara, C. Qin, A. S. Sandanayaka, C. Adachi, *Appl. Phys. Lett.* **2019**, *115*, 120601.

[22] G. Tang, P. You, Q. Tai, A. Yang, J. Cao, F. Zheng, Z. Zhou, J. Zhao, P. K. L. Chan, F. Yan, *Adv. Mater.* **2019**, *31*, 1807689.

[23] T. Yamada, T. Handa, Y. Yamada, Y. Kanemitsu,J. Phys. D **2021**, *54*, 383001.

[24] J. Ding, X. Cheng, L. Jing, T. Zhou, Y. Zhao, S. Du, *ACS Appl. Nano Mater.* **2018**, *10*, 845.

[25] D. Yue, T. Zhang, T. Wang, X. Yan, C. Guo, X. Qian, Y. Zhao, *EcoMat* **2020**, *2*, e12015.

[26] Z. Chen, B. Turedi, A. Y. Alsalloum, C. Yang, X. Zheng, I. Gereige, A. AlSaggaf, O. F. Mohammed, O. M. Bakr, *ACS Energy Lett.* **2019**, *4*, 1258.

[27] Y. Li, C. Li, H. Yu, B. Yuan, F. Xu, H. Wei, B. Cao, *Front. Chem.* **2020**, *8*, 754.

[28] S. Shahrokhi, W. Gao, Y. Wang, P. R. Anandan, M. Z. Rahaman, S. Singh, D. Wang, C. Cazorla, G. Yuan, J. M. Liu, *Small Methods* **2020**, *4*, 2000149.

[29] A. Y. Alsalloum, B. Turedi, X. Zheng, S. Mitra, A. A. Zhumekenov, K. J. Lee, P. Maity, I. Gereige, A. AlSaggaf, I. S. Roqan, *ACS Energy Lett.* **2020**, *5*, 657.

[30] D. Yan, T. Shi, Z. Zang, T. Zhou, Z. Liu, Z. Zhang, J. Du, Y. Leng, X. Tang, *Small* **2019**, *15*, 1901173.

[31] G. Tong, T. Chen, H. Li, L. Qiu, Z. Liu, Y. Dang, W. Song, L. K. Ono, Y. Jiang, Y. Qi, *Nano Energy* **2019**, *65*, 104015.

[32] M. Mehrabian, S. Dalir, G. Mahmoudi, B. Miroslaw, M. G. Babashkina, A. V. Dektereva, D. A. Safin, *Eur. J. Inorg. Chem.* **2019**, *2019*, 3699.

[33] C. Zhang, S. Wang, X. Li, M. Yuan, L. Turyanska, X. Yang, *Adv. Funct.* **2020**, *30*, 1910582.

[34] Y. Zhang, M. Lyu, T. Qiu, E. Han, I. K. Kim, M.-C. Jung, Y. H. Ng, J.-H. Yun, L. Wang, *Energies* **2020**, *13*, 4250.

[35] J. Li, L. Xu, T. Wang, J. Song, J. Chen, J. Xue, Y. Dong, B. Cai, Q. Shan, B. Han, *Advanced Materials* **2017**, *29*, 1603885.

[36] A. Z. Chen, J. J. Choi, *J. Vac. Sci. Technol. A* **2020**, *38*, 010801.

[37] X. D. Wang, W. G. Li, J. F. Liao, D. B. Kuang, *Sol. RRL* **2019**, *3*, 1800294.

[38] W. Zhang, S. Pathak, N. Sakai, T. Stergiopoulos, P. K. Nayak, N. K. Noel, A. A. Haghighirad, V. M. Burlakov, D. W. Dequilettes, A. Sadhanala, *Nat. Commun.* **2015**, *6*, 1.

[39] K. Wang, C. Wu, D. Yang, Y. Jiang, S. Priya, *ACS nano* **2018**, *12*, 4919.

[40] X. Cheng, S. Yang, B. Cao, X. Tao, Z. Chen, *Adv. Funct.* **2020**, *30*, 1905021.

[41] Z. Liu, S. P. Lau, F. Yan, *Chem. Soc. Rev.* **2015**, *44*, 5638.

[42] A. K. Geim, I. V. Grigorieva, *Nature* **2013**, *499*, 419.

[43] D. Zhao, Y. Li, *Acta Mater.* **2019**, *168*, 52.

[44] W. Mao, C. R. Hall, A. S. Chesman, C. Forsyth, Y. B. Cheng, N. W. Duffy, T. A. Smith, U. Bach, *Angew. Chem. Int. Ed. Engl.* **2019**, *58*, 2893.

[45] T. M. Brenner, D. A. Egger, L. Kronik, G. Hodes, D. Cahen, *Nat. Rev. Mater.* **2016**, *1*, 15007.

[46] M. I. Saidaminov, A. L. Abdelhady, B. Murali, E. Alarousu, V. M. Burlakov, W. Peng, I. Dursun, L. Wang, Y. He, G. Maculan, *Nat. Commun.* **2015**, *6*, 1.

[47] B. Turedi, V. Yeddu, X. Zheng, D. Y. Kim, O. M. Bakr, M. I. Saidaminov, ACS Energy Lett. **2021**, *6*, 631.

[48] A. A. Zhumekenov, M. I. Saidaminov, O. M. Bakr, World Scientific Handbook of ORGANIC OPTOELECTRONIC DEVICES **2018**, *Volume 1-Perovskite Electronics*, 241.

[49] M. Burgelman, P. Nollet, S. Degrave, Thin Solid Films **2000**, *361*, 527.

[50] A. Troisi, *Chem. Soc. Rev.* **2011**, *40*, 2347.

[51] Z. Wang, P. K. Nayak, J. A. Caraveo-Frescas, H. N. Alshareef, *Adv. Mater.* **2016**, *28*, 3831.

[52] Y. Fu, H. Zhu, J. Chen, M. P. Hautzinger, X.-Y. Zhu, S. Jin, *Nat. Rev. Mater.* **2019**, *4*, 169.

[53] J. Chen, Y. Zhou, Y. Fu, J. Pan, O. F. Mohammed, O. M. Bakr, *Chem. Rev.* **2021**.

[54] Y. Lei, Y. Chen, R. Zhang, Y. Li, Q. Yan, S. Lee, Y. Yu, H. Tsai, W. Choi, K. Wang, *Nature* **2020**, *583*, 790.

[55] D. Barrit, P. Cheng, K. Darabi, M. C. Tang, D. M. Smilgies, S. Liu, T. D. Anthopoulos, K. Zhao, A. Amassian, *Adv. Mater.* **2020**, *30*, 1907442.

[56] J. Xu, X. Li, J. Xiong, C. Yuan, S. Semin, T. Rasing, X. H. Bu, *Adv. Mater.* **2020**, *32*, 1806736.

[57] Y. Liu, Q. Dong, Y. Fang, Y. Lin, Y. Deng, J. Huang, *Adv. Mater.* **2019**, *29*, 1807707.

[58] W. Pan, H. Wei, B. Yang, *Front. Chem.* **2020**, *8*.

[59] A. Sharenko, M. F. Toney, *J. Am. Chem. Soc.* **2016**, *138*, 463.

[60] M. V. Kelso, N. K. Mahenderkar, Q. Chen, J. Z. Tubbesing, J. A. Switzer, *Science* **2019**, *364*, 166.

[61] S. Förster, K. Meinel, R. Hammer, M. Trautmann, W. Widdra, *Nature* **2013**, *502*, 215.

[62] A. Feng, X. Jiang, X. Zhang, X. Zheng, W. Zheng, O. F. Mohammed, Z. Chen, O. M. Bakr, *Chem. Mater.* **2020**, *32*, 7602.

[63] M. Ahmadi, T. Wu, B. Hu, *Adv. Mater.* **2017**, *29*, 1605242.

[64] K. Miyano, N. Tripathi, M. Yanagida, Y. Shirai, *Acc. Chem. Res.* **2016**, *49*, 303.

[65] Y.-F. Xu, M.-Z. Yang, B.-X. Chen, X.-D. Wang, H.-Y. Chen, D.-B. Kuang, C.-Y. Su, *J. Am. Chem. Soc.* **2017**, *139*, 5660.

[66] S. S. Mali, C. K. Hong, *Nanoscale* **2016**, *8*, 10528.

[67] S. Arya, P. Mahajan, R. Gupta, R. Srivastava, N. K. Tailor, S. Satapathi, S. Radhakrishnan, R. Datt, V. Gupta, *Prog. Solid. State Ch.* **2020**, 100286.

[68] F. Huang, M. Li, P. Siffalovic, G. Cao, J. Tian, *Energy Environ. Sci.* **2019**, *12*, 518.

[69] J. Li, T. Jiu, C. Duan, Y. Wang, H. Zhang, H. Jian, Y. Zhao, N. Wang, C. Huang, Y. Li, *Nano Energy* **2018**, *46*, 331.

[70] Y. Wang, J. Wan, J. Ding, J. S. Hu, D. Wang, *Angew. Chem. Int. Ed. Engl.* **2019**, *58*, 9414.

[71] S. M. Qaid, H. M. Ghaithan, B. A. Al-Asbahi, A. S. Aldwayyan, *Nanomaterials* **2020**, *10*, 2382.

[72] G. Stringfellow, *Rep. Prog. Phys.* **1982**, *45*, 469.

[73] J. Jiang, X. Sun, X. Chen, B. Wang, Z. Chen, Y. Hu, Y. Guo, L. Zhang, Y. Ma, L. Gao, *Nat. Commun.* **2019**, *10*, 1.

[74] H. Liu, in *21st Century Surface Science-a Handbook*, IntechOpen, 2020.

[75] Y. Wang, X. Sun, Z. Chen, Y. Y. Sun, S. Zhang, T. M. Lu, E. Wertz, J. Shi, *Adv. Mater.* **2017**, *29*, 1702643.

[76] M. V. Kovalenko, L. Protesescu, M. I. Bodnarchuk, *Science* **2017**, *358*, 745.

[77] H. Y. Lin, C. Y. Chen, B. W. Hsu, Y. L. Cheng, W. L. Tsai, Y. C. Huang, C. S. Tsao, H. W. Lin, *Adv. Funct.* **2019**, *29*, 1905163.

[78] C. Tan, J. Chen, X.-J. Wu, H. Zhang, *Nat. Rev. Mater.* **2018**, *3*, 1.

[79] C. Ratsch, M. Gyure, R. Caflisch, F. Gibou, M. Petersen, M. Kang, J. Garcia, D. Vvedensky, *Phys. Rev. B* **2002**, *65*, 195403.

[80] Y. Chen, Y. Lei, Y. Li, Y. Yu, J. Cai, M.-H. Chiu, R. Rao, Y. Gu, C. Wang, W. Choi, *Nature* **2020**, *577*, 209.

[81] S. Wu, R. Chen, S. Zhang, B. H. Babu, Y. Yue, H. Zhu, Z. Yang, C. Chen, W. Chen, Y. Huang, *Nat. Commun.* **2019**, *10*, 1.

[82] F. Sadeghi, M. Ashofteh, A. Homayouni, M. Abbaspour, A. Nokhodchi, H. A. Garekani, *Colloids Surf. B* **2016**, *147*, 258.

[83] T. Bu, X. Liu, J. Li, W. Huang, Z. Wu, F. Huang, Y.-B. Cheng, J. Zhong, *Solar RRL* **2020**, *4*, 1900263.

[84] C. Dong, X. Han, Y. Zhao, J. Li, L. Chang, W. Zhao, *Solar RRL* **2018**, *2*, 1800139.

[85] Z. Chen, Q. Dong, Y. Liu, C. Bao, Y. Fang, Y. Lin, S. Tang, Q. Wang, X. Xiao, Y. Bai, Y. Deng, J. Huang, Nat. Commun. **2017**, *8*, 1890.

[86] M. M. Mdleleni, T. Hyeon, K. S. Suslick, *J. Am. Chem. Soc.* **1998**, *120*, 6189.

[87] S. F. Leung, K. T. Ho, P. K. Kung, V. K. Hsiao, H. N. Alshareef, Z. L. Wang, J. H. He, *Adv. Mater.* **2018**, *30*, 1704611.

[88] J. Huang, Y. Shao, Q. Dong, X. Hu, F. Li, Y. Song, ACS Energy *Lett.* **2019**, *4*, 1065.

[89] Z. Zhang, B. Xu, B. Xu, L. Jin, H. L. Dai, Y. Rao, S. Ren, *Adv. Mater. Interfaces*. **2017**, 4, 1600769.

[90] Z. Zhang, Z. Li, S. Chang, W. Gao, G. Yuan, R.-G. Xiong, S. Ren, *Mater. Today* **2020**, 34, 51.

[91] Z. Zhang, P.-F. Li, Y.-Y. Tang, A. J. Wilson, K. Willets, M. Wuttig, R.-G. Xiong, S. Ren, *Sci. Adv.* **2017**, 3, e1701008.

[92] J. Zhao, G. Kong, S. Chen, Q. Li, B. Huang, Z. Liu, X. San, Y. Wang, C. Wang, Y. Zhen, *Sci. Bull*. **2017**, *62*.

[93] Y. Huang, T. Liu, C. Liang, J. Xia, D. Li, H. Zhang, A. Amini, G. Xing, C. Cheng, *Adv. Funct*. **2020**, *30*, 2000863.

[94] X. Tang, W. Chen, D. Wu, A. Gao, G. Li, J. Sun, K. Yi, Z. Wang, G. Pang, H. Yang, *Adv. Sci*. **2020**, *7*, 1902767.

[95] W. Gao, L. Chang, H. Ma, L. You, J. Yin, J. Liu, Z. Liu, J. Wang, G. Yuan, *NPG Asia Mater*. **2015**, *7*, e189.

[96] N. J. Jeon, J. H. Noh, Y. C. Kim, W. S. Yang, S. Ryu, S. I. Seok, *Nature Mater*. **2014**, *13*, 897.

[97] J. H. Heo, D. H. Song, S. H. Im, *Adv. Mater*. **2014**, *26*, 8179.

[98] J. Chen, D. J. Morrow, Y. Fu, W. Zheng, Y. Zhao, L. Dang, M. J. Stolt, D. D. Kohler, X. Wang, K. J. Czech, *J. Am. Chem. Soc.* **2017**, *139*, 13525.

[99] H. S. Rao, W. G. Li, B. X. Chen, D. B. Kuang, C. Y. Su, *Adv. Mater.* **2017**, *29*, 1602639.

[100] Y.-X. Chen, Q.-Q. Ge, Y. Shi, J. Liu, D.-J. Xue, J.-Y. Ma, J. Ding, H.-J. Yan, J.-S. Hu, L.-J. Wan, *J. Am. Chem. Soc.* **2016**, *138*, 16196.

[101] V. C. Nguyen, H. Katsuki, F. Sasaki, H. Yanagi, Jpn. J. Appl. Phys. **2018**, *57*, 04FL10.

[102] L. Lee, J. Baek, K. S. Park, Y.-E. Lee, N. K. Shrestha, M. M. Sung, *Nat. Commun.* **2017**, *8*, 1.

[103] Y. Fu, F. Meng, M. B. Rowley, B. J. Thompson, M. J. Shearer, D. Ma, R. J. Hamers, J. C. Wright, S. Jin, *J. Am. Chem. Soc.* **2015**, *137*, 5810.

[104] B. Li, D. Binks, G. Cao, J. Tian, *Small* **2019**, *15*, 1903613.

[105] W. Peng, L. Wang, B. Murali, K. T. Ho, A. Bera, N. Cho, C. F. Kang, V. M. Burlakov, J. Pan, L. Sinatra, *Adv. Mater.* **2016**, *28*, 3383.

[106] Y. Chen, H. Zeng, P. Ma, G. Chen, J. Jian, X. Sun, X. Li, H. Wang, W. Yin, Q. Jia, *Angew. Chem. Int. Ed. Engl.* **2021**, *60*, 2629.

[107] M. Chen, X. Shan, T. Geske, J. Li, Z.Yu, ACS Nano **2017**, *11*, 6312.

[108] S. S.Rong, M. BilalFaheem, Y.-B. Li, J. Electron. Sci. Technol. **2021**, *19*, 100081.

[109] P. Cui, D. Wei, J. Ji, H. Huang, E. Jia, S. Dou, T. Wang, W. Wang, M. Li, *Nat. Energy* **2019**, *4*, 150.

[110] Z. Fan, K. Sun, J. Wang, *J. Mater. Chem. A* **2015**, *3*, 18809.

[111] T. T. Ava, A. Al Mamun, S. Marsillac, G. Namkoong, *Appl. Sci.* **2019**, *9*, 188.

[112] E. Shi, B. Yuan, S. B. Shiring, Y. Gao, Y. Guo, C. Su, M. Lai, P. Yang, J. Kong, B. M. Savoie, *Nature* **2020**, *580*, 614.

[113] Z. Li, M. A. Najeeb, L. Alves, A. Z. Sherman, V. Shekar, P. Cruz Parrilla, I. M. Pendleton, W. Wang, P. W. Nega, M. Zeller, *Chem. Mater.* **2020**, 32, 5650.

[114] J. Kirman, A. Johnston, D. A. Kuntz, M. Askerka, Y. Gao, P. Todorović, D. Ma, G. G. Privé, E. H. Sargent, *Matter* **2020**, 2, 938.

[115] Y. Tang, Z. Li, M. A. N. Nellikkal, H. Eramian, E. M. Chan, A. J. Norquist, D. F. Hsu, J. Schrier, *J. Chem. Inf. Model.* **2021**, 61, 1593.

[116] A. A. Emery, C. Wolverton, *Sci. Data* **2017**, 4, 1.

[117] P. W. Nega, Z. Li, V. Ghosh, J. Thapa, S. Sun, N. T. P. Hartono, M. A. N. Nellikkal, A. J. Norquist, T. Buonassisi, E. M. Chan, *Appl. Phys. Lett.* **2021**, 119, 041903.

[118] E. Gu, X. Tang, S. Langner, P. Duchstein, Y. Zhao, I. Levchuk, V. Kalancha, T. Stubhan, J. Hauch, H. J. Egelhaaf, *Joule* **2020**, 4, 1806.

[119] J. C. Dahl, X. Wang, X. Huang, E. M. Chan, A. P. Alivisatos, *J. Am. Chem. Soc.* **2020**, 142, 11915.

[120] Y. Zhao, J. Zhang, Z. Xu, S. Sun, S. Langner, N. T. P. Hartono, T. Heumueller, Y. Hou, J. Elia, N. Li, *Nature Commun.* **2021**, 12, 1.

[121] E. M. Chan, C. Xu, A. W. Mao, G. Han, J. S. Owen, B. E. Cohen, D. J. Milliron, *Nano letters* **2010**, 10, 1874.

[122] J. C. Dahl, W. T. Osowiecki, Y. Cai, J. K. Swabeck, Y. Bekenstein, M. Asta, E. M. Chan, A. P. Alivisatos, *Chem. Mater.* **2019**, 31, 3134.

Halide perovskite single crystal (HPSC) films attract wide attention due to the extraordinary performance such as high carrier mobility, long carrier diffusion length, and tunable bandgap. The representative fabrication methods and characteristics, as well as the applications of typical HPSC thin films, including $MAPbI_3$, α-$FAPbI_3$, $MAPbBr_3$, $CsPbBr_3$, etc., are systematically reviewed. The prospects are also discussed at the end.

W. Gao, Z. Zhang, R. Xu, E. M. Chan,* G. Yuan,* and J.-M. Liu

Development and prospect of halide perovskite single-crystal films

ToC figure

X